IEEE Robotics and Automation Letters (RAL) paper presented at
2024 IEEE/RSJ International Conference on Intelligent Robots and Systems (IROS)
October 14-18, 2024. Abu Dhabi, UAE

Fast In-Hand Slip Control on Unfeatured Objects With Programmable Tactile Sensing

Yuri Gloumakov, *Member, IEEE*, Tae Myung Huh, *Member, IEEE*, and Hannah S. Stuart, *Senior Member, IEEE*

***Abstract*—Accurate dynamic object manipulation in a robotic hand remains a difficult task, especially when frictional slip is involved. Prior solutions involve extensive data collection to train complex models to control the hand that do not necessarily generalize to other slip circumstances. Our approach focuses on direct slip sensing using a tactile sensor with a capacitive array, coupled with a programmable system on a chip, capable of mode switching and sampling rate adjustment. We characterize the sensor's capacity to sense slip features at higher speeds and introduce a novel methodology for estimating motions. Low-level sensor reprogramming that couples multiple taxels improves slip avoidance and reaction time during rapid slip onset events. The technology also tracks dominant surface vibration frequencies resulting from stick-slip cycles, estimating speed and acceleration of smooth flat surfaces. Using a parallel-jaw robotic gripper, we demonstrate dynamic repositioning of objects lacking trackable surface features within the hand. The goal of this investigation is to support faster reasoning and reflexes for dynamic dexterous robots that experience directional in-hand slip.**

***Index Terms*—Force and tactile sensing, in-hand manipulation, perception for grasping and manipulation.**

I. Introduction

ROBOTIC within-hand manipulation [1] can significantly enhance the capability of robots to execute tasks that would otherwise be too difficult to accomplish, yet it continues to face substantial challenges [2]. Enabling object reorientation within the gripper, for instance, facilitates the repositioning of items in constrained spaces where broad arm movements are impractical. Achievements in this area have leveraged controlled slippage [3], provided slip is not catastrophic and object dynamics, such as velocity, can be reliably estimated. Uncertainties in object properties that make it difficult to predict in-hand slip, such as mass and friction, has led some efforts to constrain the object to slip in simple and predictable ways [4]. However, following predefined trajectories is not always possible or preferable, and in dynamic within-hand manipulation scenarios precise object models are often necessary to predictably accomplish tasks [5]. Other efforts have identified regions of the hand workspace where drops are likely, both in robot [6] and human [7] manipulators, in an effort to avoid those regions entirely.

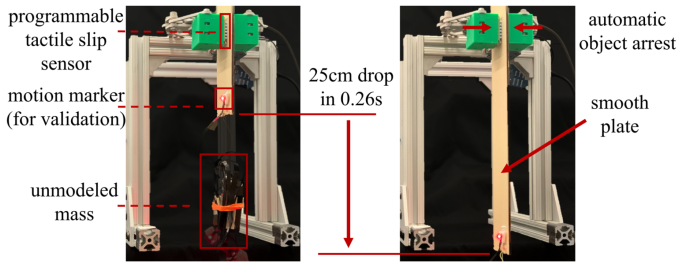

Fig. 1. High-speed in-hand repositioning facilitated by SlipTack, capable of accurately estimating slipping object acceleration.

Tactile sensing can enable robots to detect incipient slip and prevent object drops [8] and is one way to control frictional slipping behaviors purposefully. However, without knowing precise object properties, tracking object features (such as edges), using external constraints, or relying on computer vision, the only way left to estimate slipping motion is through the dynamic friction interaction between the object and sensor. By relying solely on the dynamic friction interaction, we aim to develop generalizeable manipulation capabilities that more closely resemble our own. It is our goal to control slip using tactile sensing during especially agile, or fast, in-hand manipulations for less structured tasks. For example, as seen in Fig. 1, a parallel-jaw gripper estimates the motion of an object as it slips at 7.0 m/s^2 in the hand, then, via acceleration integration, the object is automatically stopped after 25 cm of travel.

In this work, we conduct slip sensing using a previously developed capacitive, geometrically featured, low-cost tactile sensor, whose parameters and function is described in detail in [9], herein referred to as SlipTack (manufactured by the authors). While prior work demonstrated its low-level functions, especially the ability to discern slip directions on featureless surfaces, these tests were intentionally performed at robot speeds of $\leq$10 mm/s without estimating object velocity or acceleration or rapid onset slip events. To improve the practicality of the sensor and support agile manipulation, our contributions are as follows: for the first time *(1)* we validate that a model-based

Manuscript received 18 March 2024; accepted 23 April 2024. Date of publication 13 May 2024; date of current version 20 May 2024. This letter was recommended for publication by Associate Editor R. Liu and Editor A. Banerjee upon evaluation of the reviewers' comments. This work was supported by the InnoHK of the Government of the Hong Kong Special Administrative Region through the Hong Kong Centre for Logistics Robotics. *(Corresponding author: Hannah S. Stuart.)*

Yuri Gloumakov and Hannah S. Stuart are with the Embodied Dexterity Group, Department of Mechanical Engineering, University of California Berkeley, Berkeley, CA 94720 USA (e-mail: hstuart@berkeley.edu).

Tae Myung Huh is with the Department of Electrical and Computer Engineering, University of California Santa Cruz, Santa Cruz, CA 95064 USA.

There is a supplemental video associated with this work.

This letter has supplementary downloadable material available at https://doi.org/10.1109/LRA.2024.3400148, provided by the authors.

Digital Object Identifier 10.1109/LRA.2024.3400148

approach can sense object velocity up to 100 mm/s, *(2)* characterize object acceleration and demonstrate dynamic in-hand object repositioning via integration, and *(3)* highlight the benefits of sensing modularity for rapid slip detection for suppression reflexes and object stabilization. These demonstrations suggest principles for future sensors, where the addition of tactile geometric features coupled with modular sensor design enables switching to simpler, yet faster, sensing modalities.

A. Overview

We review the state of the art for in-hand slip sensing (Section II), highlighting the challenges of handling smooth, or *unfeatured*, objects quickly. We describe the capacitive programmable SlipTack and the principles that govern the tactile signal (Section III). Methodology for data collection, slip speed and acceleration estimation, and dynamic manipulation experiments are outlined (Section IV), followed by results (Section V). We conclude with a discussion (Section VI) and propose future work (Section VII).

II. Related Work: In-Hand Slip Sensing

Agile slip sensing, quick relative motion detection and data transmission, is imperative to observe dynamic manipulation or avoid dropping objects. Tactile sensors optimized for transmitting high spatial resolution touch data at low frequencies (30–100 Hz)[1] may not be well suited for these tasks. Designing separate sensors for specific attributes, at the cost of greater information resolution, enables higher transmission rates better suited for reducing delay in high-frequency vibration detection during frictional slip. For reference, human skin can detect frequencies up to 400 Hz [10].

A. Inferring Slip From High Resolution Data

Tactile sensing research often focuses on high-resolution vision-based sensors like GelSight for detecting geometric contact features [11]. GelSight has been applied to slip detection [12] and object pose moderation during slip manipulations [13]. However, finger cameras have limited sensing rates ($\sim$30 Hz), making them less suitable for fast slip onset detection or dynamic manipulation compared to sensors using faster-sampling transduction technologies like pressure [14] or acceleration [15]. Proposed neuromorphic approaches aim to address the sampling rate shortcomings [16]. Concerns with vision-based sensors include bulk [17] and being limited to sensing pressure distributions due to a simple uniform tactile surface. In other words, it works best when there's a trackable geometric feature on the object in contact with the finger. Despite attempts to enhance sensing resolution, even in non-vision-based sensors, they continue to lack the capacity to characterize the slip of smooth flat objects.

B. Slip Characterization With High Sensing Rates

In prior research, an accelerometer embedded in a rubber skin was found to distinguish low from high speeds of sliding objects while attempting to detect object textures [18]. Recent tactile sensors directly measure object slipping speed by timing its edge passing over two known features on the sensor (e.g. [19], [20]). In sensors with uniformly spaced geometrical features, the dominant frequency in the signal's spectrogram has also been used to determine the rate of interaction with each additional feature [21]. We propose that a similar approach could be used to identify stick-slip oscillations of tactile features, enabling the detection of slipping speed for objects in flush contact with the sensor.

Slip speed has also been indirectly tracked using precise dynamic models [22] or highly parametric models trained with data that appears to generalize [23]. However, neither method uses simple and predictable models to directly observe the sliding interaction as we do here. Prior studies have utilized geometric features to detect incipient slip by analyzing surface vibrations [24] and distinguishing between slip occurring with respect to the hand or the environment [25]. Directly detecting object slipping speed has not been achieved for objects that lack detectable features, such as planks or boxes.

C. Leveraging Slip for Object Manipulation

In practice, dynamic manipulation necessitates object acceleration and deceleration, and incipient slip and speed tracking alone may not be sufficient. Friction cones can estimate object sliding and facilitate planning for in-hand object repositioning [26]. When object properties are unknown, friction cones can be also be used in conjunction with proprioception to slide objects along a table [27]. Successful within-hand object repositioning has been achieved when external cameras are available [28] or when objects have well-defined geometries trained with real-world [29] or simulated [30] object contacts. These methods can fail when handling objects that are flush with the sensor and occluded from vision.

When dealing with objects without well-defined geometries, solely relying on tactile information to controllably regrasp an object has only been accomplished with highly parametric pretrained models [23]. Therefore, our final goal is to demonstrate that SlipTack can also estimate slip acceleration by sensing the energetics of a slipping event. We showcase within-hand object repositioning by effectively stopping a slipping object at a desired position using a simple model, without relying on external sensing.

III. Programmable Slip Tactile Sensor

We use SlipTack (Fig. 2) to demonstrate for the first time the principles proposed in Section I. The remainder of this section presents models that inform sensing characterization.

A. Object Slipping At Steady-State Speed

For this section we assume that a simple stick-slip friction oscillator model [31] dominates the interaction at the interface between the objects and the sensor surface. We model stick-slip using normal load F_n, lateral spring stiffness k_l, static friction coefficient μ_s, kinetic friction coefficient μ_k (where $\mu_k < \mu_s$), constant pulling speed v_0, nib mass M, and relative nib displacement u (Fig. 3(a)). The static friction keeps the nibs in

[1]Sample transmission rate is typically lower than maximum detectable transducer frequency. For example, a strain sensor can detect signals over 1 kHz, however the data transfer rate to the robot controller isn't this high.

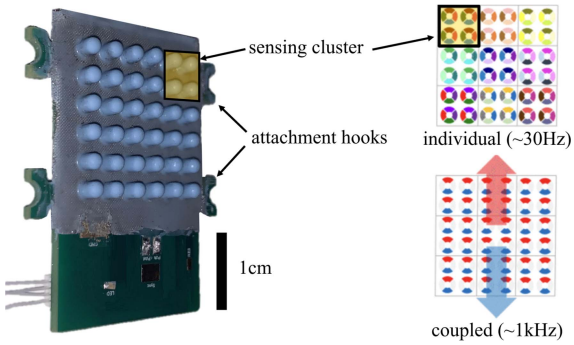

Fig. 2. The surface is discretized to nine sensing clusters, each detecting deflection of the features along the four cardinal directions. Sensing clusters can be coupled in various configurations to focus the sensing on particular interactions. Colors illustrate individual capacitive transducers that are electrically coupled or decoupled to get different programmable configurations. Attachment hooks assist in aligning and physically securing the sensor to robotic fingers used in this work. Image adapted from [9].

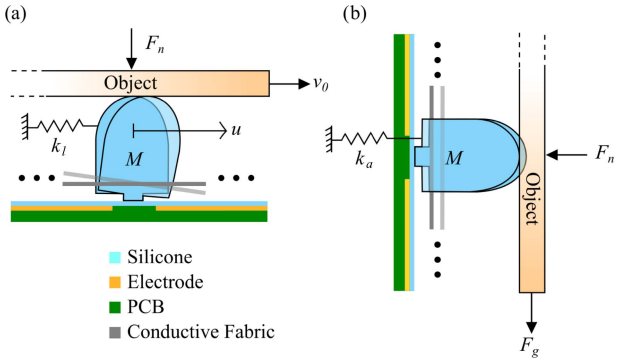

Fig. 3. Force diagram of a nib undergoing (a) a stick-slip interaction with an object being pulled laterally and (b) an accelerating sheering motion due to a dropping object.

'stick' phase while $\mu_s F_n \geq k_l u$, where nib speed $\dot{u}$ is equal to object speed v_0. Nibs begin to slip when u is large enough to induce a spring force that overcomes the static friction force, $\mu_s F_n = k_l u$. When the nibs begin to slip relative to the object, i.e. 'slip' phase, we obtain the following equation of nib motion and its solution:

$$M\ddot{u} = \mu_k F_n - k_l u \tag{1}$$

$$u = A\sin(\omega_0(t-\tau)) + \mu_k F_n / k_l \tag{2}$$

where natural frequency $\omega_0 = \sqrt{k_l/M}$ is a function of nib geometry and material properties and amplitude A and phase τ are determined by the initial conditions. The nibs will continue to slip until relative velocity $(\dot{u} - v_0)$ returns to zero, where adhesion is regained and the 'stick' phase starts again. Alternating between 'stick' and 'slip' results in a periodic motion whose frequency increases with increasing v_0 until saturation [32], during which the period will resemble the natural frequency. Frequency, f, is related to pull speed, v_0, as follows:

$$f = 1/(\tau_{stick} + \tau_{slip}) \tag{3}$$

where $\tau_{stick} = (\mu_s F_n)/(k_l v_0)$ and $\tau_{slip} = \pi w_0/2$ correspond to the time the sensor is in the stick and slip phases, respectively. Stick-slip frequency will saturate at lower v_0 with nibs that have a higher natural frequency or with materials that exhibit a smaller difference between the static and kinetic friction coefficients.

B. Object Acceleration

By adjusting grip force and leveraging gravity for acceleration, a quick reposition can be achieved with minimal movement. Downward object acceleration, a, may be estimated by experimentally calibrating sensor values to measure axial nib displacement, $x - x_0$ (akin to tracking F_n) (Fig. 3(b)):

$$a = g - \frac{1}{m_t}\mu_k k_a (x - x_0) \tag{4}$$

where g is the gravitational constant, m_t is the total mass of the object and attached weight, and k_a is the axial spring stiffness of the surface. Acceleration may also be estimated by tracking the slope of the frequency response: if f_t (from (3)) corresponds to speed at time t, then,

$$a = (f_{t2} - f_{t1})/(t_2 - t_1) \tag{5}$$

Both approaches aught to closely estimate acceleration. To minimize the estimation time and enable a larger range of regrasping positions, we use the calibrated model to perform a dynamic regrasping demonstration in Section IV, where we estimate $(x - x_0)$ using the sensed deflection.

C. Sensing Modes and Sampling Rate

With limited bandwidth, sensors have to be pre-selected with desired characteristics related to resolution and sensing frequency. SlipTack is capable of altering its sensing modality in real-time using Programmable System on Chip (PSoC) architecture, leveraging the integrated analog multiplexers to electrically connect multiple tactile sensing pixels, or taxels, by the program. This flexibility enables us to sample at a lower rate (*individual* mode, $\sim$30 Hz) with high spatial resolution or at much higher rates (*coupled* mode, $\sim$2 kHz) for a particular direction of interaction by coupling various capacitive elements to downsize the information packet (Fig. 2). For example, the tactile features can be coupled to sense along the four cardinal directions at $\sim$500 Hz when the interaction event is linear or along clockwise direction at $\sim$1 kHz when the event is expect to be rotational. In the majority of our experiments, we utilized the fastest $\sim$1 kHz coupled mode for linear motion to measure the largest range of slip vibration frequencies.

IV. Methods

Our goal is to experimentally test two potential SlipTack capabilities: ability to detect the speed of a slipping unfeatured object and estimate its acceleration. We establish a parametric relationship between the signals captured by SlipTack and the speed and acceleration of slipping objects.

A. Sensor Hardware Integration

In the speed trials, SlipTack was placed in a clasp that kept a constant distance between the sliding object and the sensor's surface while ensuring that the two surfaces were flush. A precise pull motion was made possible using a UR-16 robot arm (Universal Robots, Denmark) with a customized end-effector

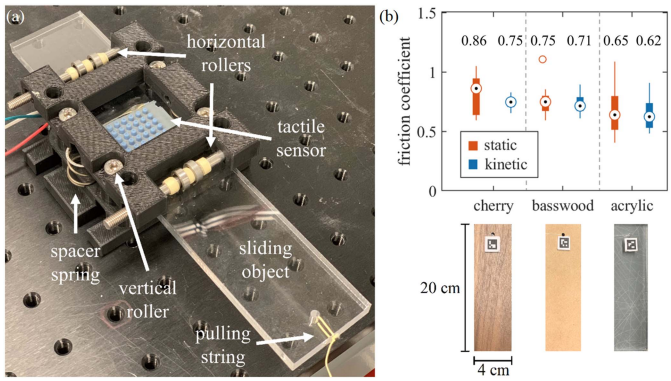

Fig. 4. (a) A custom clamp is affixed to the table that is set to maintain a constant maximum distance between the object and the tactile sensor. A cutout is included at the top of the clamp so that the interaction can be visually observed. Vertical and horizontal rollers ensure that the objects slide along a straight line. (b) Mean (displayed) and interquartile ranges of measured static and kinetic friction coefficients of the three tested objects.

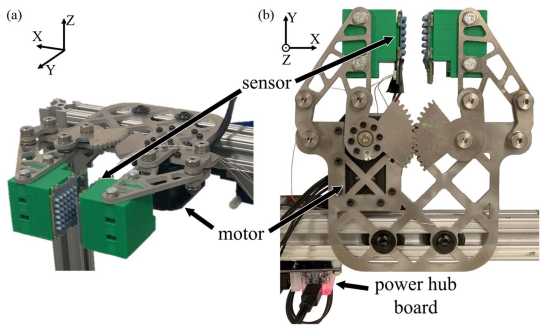

Fig. 5. (a) Side view of the parallel-jaw gripper and its components. (b) Top-down view of the gripper.

and a string (Fig. 4(a)). For acceleration trials, two sensors (only one is used for sensing) were placed on a custom-built 1-DOF parallel-jaw gripper made of 0.125" aluminum and 3D-printed PLA fingers (Fig. 5) driven by a Dynamixel MX-28R motor (ROBOTIS, South Korea). Grasp aperture resolution of this gripper was limited by motor specifications and finger geometry, and was discretized according to $L\cos\theta_m$, where θ_m is the motor angle and L is the length of the finger in the parallel mechanism. Since the resolution of $\theta_m = 0.09°$, the resolution of the gripper fingertip in the region of interest was approximately 0.3 mm.

B. Test Objects

The study used objects laser-cut from cherry, basswood, and acrylic. The selection aimed to represent variations within and between material categories, such as wood-to-wood and wood-to-acrylic, rather than being exhaustive. Static and kinetic friction coefficients were obtained by mounting the sensor on a reference Axis80-M8 force/torque sensor (ATI Industrial Automation, USA) and dragging it across the different surfaces using the UR-16 arm. The results in Fig. 4(b) represent 15 trials each; 5 trials at 2, 3, and 4 N of normal force with a displacement of 4 cm horizontally over the course of 1 s. For the speed and acceleration trials, object dimensions were $0.32 \times 4 \times 20$ cm

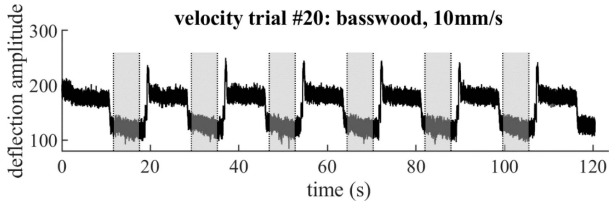

Fig. 6. Example velocity trial. Sensor amplitude can be seen going through push and pull phases. Acceleration and deceleration are omitted when splicing the steady state pull regions (highlighted).

and $0.32 \times 6 \times 50$ cm, respectively. Different sizes were used to suit different test setups; a longer object for acceleration trials provided more time before it escaped the grasp. A string is attached to the bottom of each object for the robot arm to pull during speed trials or add weight for additional downward force in acceleration trials.

C. Speed Trials and Analysis

Objects were pulled at 10–100 mm/s in increments of 5 mm/s across the sensor. The arm accelerated to a desired speed while the string was slack. The end-effector was then used to push (i.e. reset) the objects back into place. Cycling between pulling and pushing lasted for 2 minutes.

The sensor data collected during speed trials was first segmented to remove periods of acceleration, deceleration, and object resetting, as illustrated in Fig. 6. Each pull cycle was then converted to the frequency spectrum using discrete Fourier transform with a Hamming window filter. The average of 300-frame moving window was subtracted from the data to eliminate low frequencies associated with gross displacement. For each pull cycle, a frequency spectrum was obtained, and the average dominant frequency is acquired using a bootstrap calculation. This calculation considers different ways of obtaining the proxy dominant frequency, with the number of peaks used ranging from 1 to 10. The final dominant frequency (f_d) is obtained by taking the mean of the individual dominant frequencies (f_i) across different frequency ranges:

$$f_i(f_{\max}) = \left(\sum_{j=1}^{10} \frac{\sum_{k=1}^{i} p(k, f_{\max})}{j} \right) /10 \tag{6}$$

$$f_d = \left(\sum_{f_{\max}=15}^{40} f_i \right) /26 \tag{7}$$

where p refers to a sorted list of peaks based on amplitude. The frequency spectrum was limited to $f_{\max}$, ranging in 15–40 Hz to exclude harmonic frequencies but large enough to include relevant frequency signals; stick-slip oscillations are expected to be within that range [9].

D. Acceleration Trials and Analysis

In our robotic gripper, the desired inter-finger gap distance d was selected within the bounds of $[d_{\min}, d_{\max}]$. $d_{\min}$ was designated to prevent device damage while preventing object slipping, while $d_{\max}$ was the largest distance where the fingers are still applying a friction force F_f preventing object free-fall.

During data collection and manipulation trials, d was initially set to $d_{\min}$ to preload the object in the fingers. By varying d within the range $[d_0, d_{\max}]$ we applied different amounts of normal force F_n, and thus induced different downward accelerations. d_0 is the position value where the resulting F_f is equal to the force due to gravity F_g, corresponding to an object slipping at constant speed. Due to different friction properties between objects, this resulted in slightly different grasping ranges. Each position d was repeated 5 times. Ground truth data was collected using Impulse X2E Motion Capture system (PhaseSpace, San Leandro CA, USA), recording at 240 Hz with $<$1 mm precision. An LED was attached to the base of the basswood object increasing its weight by 15 g; the weight is due to the LED cluster and transmitter that had to also be attached to keep the object freestanding. Along with an added 200 g weight, the total object weight was 283 g.

The object is set up vertically, with the robot fingers pinching the bottom of the object (Fig. 1), with the weight stationary prior to release. Non-idealities causing horizontal motion during slip are ignored; horizontal deflections were on average 11% of the total vertical deflection. Object position data was first filtered using a 10-frame moving average before calculating the frame-by-frame acceleration. Due to the non-linear and unpredictable interaction of the object and sensor at the instance of release, a representative object acceleration was obtained after 0.06 s of its release up to 15 cm of the object's travel.

Over the same period, the sensor output a signal corresponding to the linear deflection along the sliding direction. Signal features included the gross and net amplitude change of the normal and tangential deflection as well as characteristics of the signal in the frequency domain. The frequencies were obtained by converting a moving 300-frame window using a Fourier transform, and the time-evolving spectrogram was characterized to a single value in a variety of exploratory ways. At each time step, the frequency bins were summarized as one of the following: maximum frequency, weighted or un-weighted mean of the top 5 frequencies, mean frequency amplitude, or maximum frequency amplitude. As the signal evolved over time, the signal was simplified by a mean, maximum, or slope to yield a single representative value. In total, there were 10 signal interpretations, 1 that is related to the gross deflection amplitude (G), and 9 obtained from the frequency domain: mean-mean of the amplitude (MM), mean of the peak amplitude (MP), weighted mean frequency (MF), peak of the mean amplitude (PM), peak of the peak amplitude (PP), peak frequency (PM), slope of the mean amplitude (SM), slope of the peak amplitude (SP), and slope of the mean frequency (SF). We then compare these features using principal component analysis (PCA) and a biplot; exploratory techniques that help identify patterns and relationships in multivariate data.

E. Regrasping Demonstration

We demonstrate two dynamic autonomous robotic behaviors performed using SlipTack signals. The first leverages the estimated acceleration regression model, obtained experimentally, to dynamically reposition the basswood object. The objective is to discover if the relationship between the sensor and acceleration can be put to practical use in a real system and evaluate its limitations.

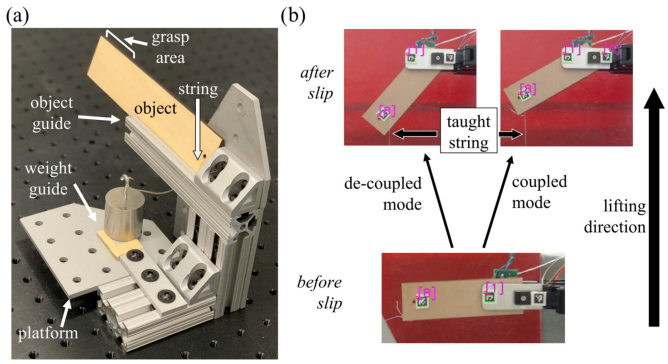

Fig. 7. (a) Fixed guides used to replace the weight and objects in consistent locations. (b) Example of a start and end object position within the robotic hand during the lifting trials. Trials differed only in slip sensing modality.

We used the same gripper setup as in Fig. 5. The demonstration utilized a Python script that interpreted the sensor signals over a 0.03 s period and determined gripper open duration to achieve desired slip distance. Considering the 0.12 s nominal motor response time, regrasping locations had to account for inadvertent displacement during finger closure. Here, we attempt to regrasp the object after 20, 25, and 30 cm of vertical translation while varying the grasping force to induce different accelerations. Each grasp force and desired displacement trial was repeated five times. Motion capture was used to track objects' ground truth displacements solely to quantify the model's accuracy.

F. Slip Arrest Demonstration

The second demonstration explores our assumption and aims to demonstrate that sensing modularity, and thus data collection speed, enables meaningfully faster reactions to the onset of slip, in particular when the interaction is known in advance. As discussed in Section II, binary slip detection for object arrest has been shown to be useful in prior work. In Section III, we discuss how SlipTack's sampling frequency can be adjusted by coupling the sensing elements and reducing the information resolution, yet until this point, we assume throughout our experiments the fastest sampling rate at all times. We now confirm this assumption using slip avoidance trials at different sensing rates, in which SlipTack is placed on one finger of a commercially available 1-DOF 2F-140 parallel-jaw gripper (Robotiq, Quebec, Canada).

Torsional slip was induced by a sudden downward force on one end of an object using a string and a weight, simulating events such as snagging or non-uniform objects [33]. The basswood object[2] was placed horizontally on its edge using a guide (Fig. 7) to ensure that it was grasped in the same location (other end of the object) each time. The guide was also used to precisely reset the location of the weight, such that the direction of the downward force was consistent between trials. The Robotiq gripper, on the UR-16 robot arm, first grasped the object at one end. It then moved it to a location such that the string at

[2]The object is now shorter ($0.32 \times 4 \times 13$ cm) to reduce inertial effects.

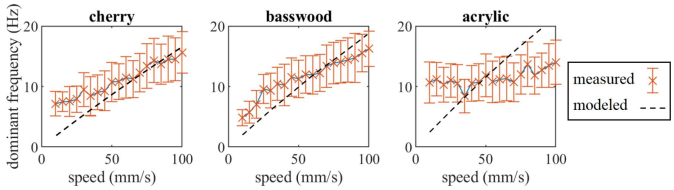

Fig. 8. Dominant frequency, both experimental (crosses) and modeled (dashed line), is plotted against the speed of the sliding object.

the other end was directly above the attached weight. A desired finger opening distance d was selected within the bounds of $[d_{\min}, d_{\max}]$, however, unlike in Section IV-D, $d_{\max}$ was set in the range where rotational slipping can occur when the impulse occurs, while avoiding being too large for translational slip [28].

The arm was programmed to accelerate to 3 m/s before the string became taught. The weight would then induce an instantaneous downward force causing the object to slip. The sensor's signal was converted to the frequency domain, and when torsional slip was detected, the gripper was commanded to close in order to increase the normal force and arrest the object. Slip detection was based on prior work that found the effective frequency response to be $\sim$10 Hz [9]. The individual and coupled modes were each tested over 30 trials. Reaction time was quantified by object rotation. Aruco markers on the gripper and object recorded rotational slip in degrees.

V. Results

Speed estimation: The dominant sensor frequency, obtained using (7), is plotted against the object pull speed (Fig. 8). The standard deviations indicate a substantial variation in the signal, however, a trend can nonetheless be observed for two of the three tested objects. The prominent frequency did not exhibit a consistent trend in the acrylic material, and could be a nonlinear interaction due to adhesion between the acrylic and the sensor's silicone surface. Such factors appear to pose a potential limitation of the stick-slip model described in Section III-A. The dominant frequency did not appear to saturate with increasing sliding speed for the cherry and basswood materials, meaning that SlipTack is capable of sensing higher slipping speeds for those materials. Theoretical model is additionally included based on (3) using the sensor's parameters.[3]

Acceleration estimation: An example trial is displayed in (Fig. 9), where the sensor signal and the ground truth object dynamics are displayed. Missing position data can be seen near 2.5 s and occurs after the object leaves the gripper.

Variables related to acceleration (AM) and sensor data are projected to the first two principle components, which are the two that account for the most variation in the data (Fig. 10). A biplot was then used to reduce the number of variables and decrease sparsity. The analysis revealed that the variables that most closely correlated with acceleration (AM) did not include frequency slope (SF), but rather signals related to amplitude (G, MM, MP, PM, and PP). Acceleration (AM) is plotted against the signal's gross deflection amplitude (G) (Fig. 11) and the linear regression model (calibration) is then used to estimate the acceleration of the slipping objects in the following regrasping experiments. Future improvements may enable the use of SF under more ideal conditions.

A weaker correlation between sensor signal and acceleration was detected for the acrylic than for the other materials (Fig. 11), but was stronger than the correlation between its signal and

[3]Individual nib mass M = 1.4e-5 kg and k_l = 9.45 N/m.

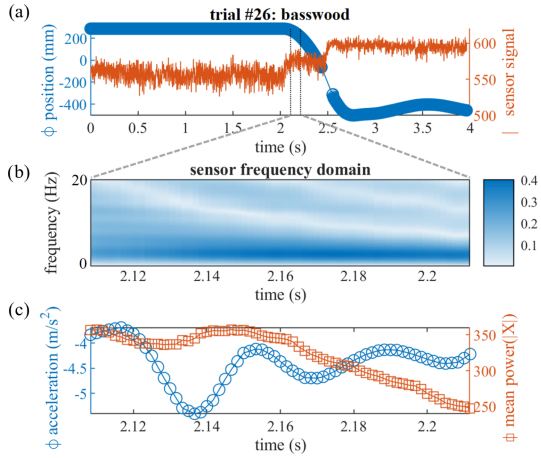

Fig. 9. Example data obtained from a single drop trial. (a) Ground truth position data (left y-axis) is obtained using motion capture. Sensor signal (right y-axis) refers to the difference between the summed up/down capacitor values. Vertical lines define the region that is used for relating acceleration to sensor data. (b) Sensor signal in the range of interest is displayed in the frequency domain. (c) Variation in acceleration (left y-axis) is due to a non-linear interaction between the sensor and object. Mean power spectrum density (right y-axis) is obtained by taking the mean amplitude of the frequency signal in the 0–20 Hz range.

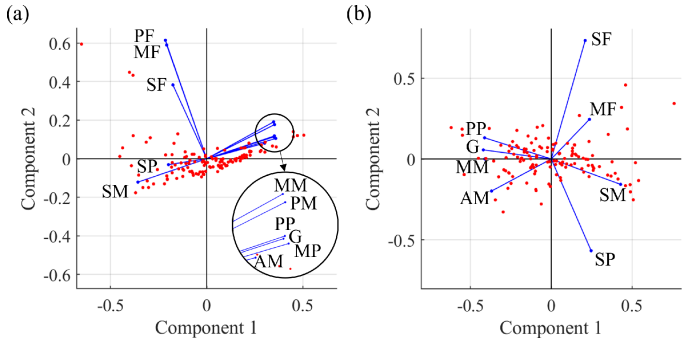

Fig. 10. Biplot analysis of sensor features and motion capture data. (a) All variables are included in the first model. (b) Highly similar features were removed, improving sparsity.

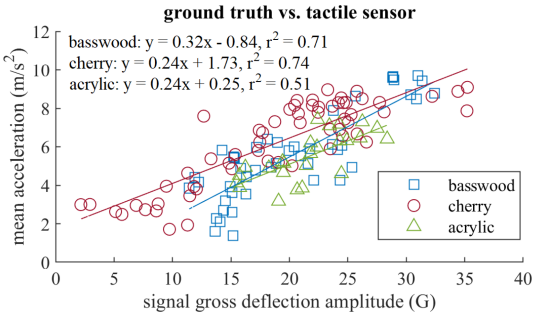

Fig. 11. Comparing the observed ground truth mean acceleration (AM) with the sensor's gross deflection amplitude (G).

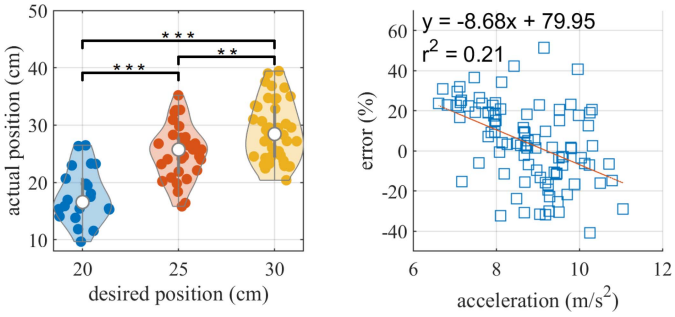

Fig. 12. (a) Results demonstrating the performance of the regrasping demonstration, where we varied the desired position. (b) Regrasp position error is largely invariant with the induced acceleration. Two-way t-test: $^{**}p < 0.01$, $^{***}p < 0.001$.

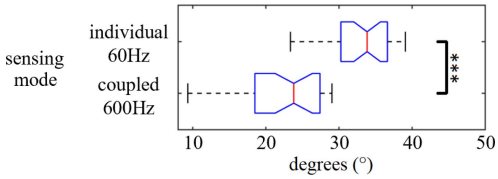

Fig. 13. The notched box plots summarize the amount of rotations the objects have undergone prior to slip arrest. $^{***}p < 0.001$.

speed. This is likely due to the use of gross nib deflection to estimate acceleration, which was less dependent on stick-slip interaction that was used to estimate speed. Nonetheless, large variance remains, and it is not yet clear how this would affect real-world manipulation accuracy.

Regrasping demonstration: Fig. 12(a) compares the actual position achieved to the desired position. The demonstration resulted in dynamic repositioning actions with an overall accuracy error of 19.7% across all trials, which is within the error range of even works using external cameras [28]. Despite the seemingly large variance, a one-way ANOVA has determined that the desired position has a statistically significant impact on the final position ($p < 0.001$). As seen in Fig. 12(b), the different gripper opening behaviors resulted in a range of real object accelerations.[4] Importantly, reposition error only weakly correlated with the induced acceleration, i.e. regrasping performance is acceleration invariant, suggesting the variance is due to external factors such as errors in sensor manufacturing. This indicates that the gripper is autonomously adapting it's behavior effectively to the variability in grasping force even as acceleration doubles.

Slip arrest demonstration: Reaction time was quantified by object rotation. Due to a faster sampling rate (600 Hz vs. 60 Hz), the coupled mode was expected to detect slip 0.015 s sooner than the individual mode, improving slip arrest by up to $\sim 20^\circ$. In practice, coupling sensing channels prevented an average of 10° of additional slip (Fig. 13). A paired-sample t-test showed significant differences in slip detection between the two modes ($p < 0.001$), with non-overlapping notches indicating differing true medians with at least 95% confidence. In the accompanying media attachment, we demonstrate similar slip arrest performance differences using a box with unknown weight.

[4]Note that some of the trials had an estimated acceleration beyond the expected 9.8 m/s^2, which we attributed to ground truth sensing noise, and contributed to the regrasping error. Similarly, we omitted data if the motion capture system was erroneous or lost during these trials.

VI. Discussion

This study established correlations between sensor signal and slipping object dynamics. Stick-slip oscillations correlated with sliding speed for two of the three tested objects. The interaction between acrylic and the sensor's silicone surface defied estimation using a simple friction model. Unaccounted factors, such as viscous friction and inelastic deformation, contributed to signal variance. We suspect that surfaces like cardboard or paper [18] may exhibit similar behavior to the wood materials in this study. To generalize this concept, there appears to be a subset of surface types that are uniquely positioned to relay stick-slip information when interacting with SlipTack. This model could also be applied to other geometrically featured sensors, albeit with variable sensing accuracy depending on material selection.

We established linear relationships between sensor signals and acceleration across the different signal interpretations, with certain frequency domain interpretations closely linked to gross deflection amplitude. This is likely due to accelerating nib deflections dominating any oscillating signal from stick-slip friction. The frequency spectrum, requiring more sensing time for acceleration interpretation than gross deflection, is useful for a narrower range of object reposition locations; the object would need to slip further in order to control it accurately, and is why we proceeded to implemented gross deflection in tracking acceleration in the manipulation tasks. We will show in future work how acceleration in less aggressive interactions may be detected using the changing frequency signal over time, while also showing how this concept works with other geometrically featured sensors.

For the dynamic within-hand manipulation demonstration, we successfully regrasped the object at three locations 5 mm apart with statistical significance. The lack of a significant relationship between acceleration and error suggests that acceleration was accounted for during the repositioning tasks. This functionally meaningful outcome is notable given the wide characterization variability observed in the acceleration to signal correlation.

The slip avoidance demonstration emphasized the advantages of adjustable sensing modes, showing that SlipTack rates significantly impact reaction times and slip distances. Dedicated sensing modes improve reaction time, particularly in tasks with predictable dominant interactions, as seen in this study where we anticipated specific motions based on the experimental setup. This allowed us to measure linear or rotational slip at the maximum frequency. In addition to enabling faster sampling rates, coupling the capacitive array using the integrated analog multiplexer also had the benefit of acting as a low-pass filter.

A. Future Work

It is expected that new sensing modes may be needed to optimize performance when handling other materials in more complex ways, for example, when handling small or irregular objects. In the future, we will characterize and showcase regrasping with rotating objects, like executing a swing-up motion (as in [30]).

A stiffer nib design could reduce signal noise but would increase resonant and stick-slip frequencies, demanding higher sampling rates to avoid aliasing. SlipTack, with a resonant frequency of ~ 10 Hz, can presently sample upward of 2 kHz in the most simple sensing case, meaning that there is flexibility to either decouple the taxels to sense more complex interactions or have a stiffer surface to reduce contact interaction noise. However, stiffer nibs might also reduce the displacement of the conductive fabric layer, potentially lowering sensitivity. Modularity is even more important if looking to scale SlipTack to larger surfaces, which may require using different capacitive element sizes/patterns or multiple distributed sensing circuits, without which sensing would be limited by sample rates.

After repeated testing, SlipTack's surface showed wear, introducing noise, and in the worst case, peeled off of the PCB, necessitating the replacement of the entire sensor. While this occurred after extensive sliding and impulse trials with various frictional loads, future work could further ruggedize the skin. The sensor was replaced after each trial block, exhibiting wear from both speed and acceleration trials and peeling during the slip reaction trials. Nevertheless, we expect the established principles in this work to apply to other new sensor designs.

VII. Conclusion

When seeking to control fast in-hand slip maneuvers, especially on unfeatured objects, programmability of the tactile sensing modality enables higher data rates and faster reflexes. Specifically for SlipTack, speed and acceleration estimation is a promising pathway for moving beyond binary slip detection to slip control. Ultimately, similar dynamic tactile sensing technologies will allow robots to more accurately operate at higher speeds in unstructured tasks.

References

[1] A. Bicchi, "Hands for dexterous manipulation and robust grasping: A difficult road toward simplicity," *IEEE Trans. Robot. Automat.*, vol. 16, no. 6, pp. 652–662, Dec. 2000.

[2] J. Bohg, A. Morales, T. Asfour, and D. Kragic, "Data-driven grasp synthesis–A survey," *IEEE Trans. Robot.*, vol. 30, no. 2, pp. 289–309, Apr. 2014.

[3] J. W. James and N. F. Lepora, "Slip detection for grasp stabilization with a multifingered tactile robot hand," *IEEE Trans. Robot.*, vol. 37, no. 2, pp. 506–519, Apr. 2021.

[4] W. G. Bircher, A. S. Morgan, and A. M. Dollar, "Complex manipulation with a simple robotic hand through contact breaking and caging," *Sci. Robot.*, vol. 6, no. 54, 2021, Art. no. eabd2666.

[5] N. C. Dafle et al., "Extrinsic dexterity: In-hand manipulation with external forces," in *Proc. IEEE Int. Conf. Robot. Automat.*, 2014, pp. 1578–1585.

[6] A. S. Morgan, W. G. Bircher, and A. M. Dollar, "Towards generalized manipulation learning through grasp mechanics-based features and self-supervision," *IEEE Trans. Robot.*, vol. 37, no. 5, pp. 1553–1569, Oct. 2021.

[7] Y. Gloumakov, T. Feix, I. M. Bullock, and A. M. Dollar, "Object stability during human precision fingertip manipulation," in *Proc. IEEE Haptics Symp.*, 2016, pp. 84–91.

[8] W. Chen, H. Khamis, I. Birznieks, N. F. Lepora, and S. J. Redmond, "Tactile sensors for friction estimation and incipient slip detection–Toward dexterous robotic manipulation: A review," *IEEE Sensors J.*, vol. 18, no. 22, pp. 9049–9064, Nov. 2018.

[9] T. M. Huh, H. Choi, S. Willcox, S. Moon, and M. R. Cutkosky, "Dynamically reconfigurable tactile sensor for robotic manipulation," *IEEE Robot. Automat. Lett.*, vol. 5, no. 2, pp. 2562–2569, Apr. 2020.

[10] R. S. Johansson and J. R. Flanagan, "Coding and use of tactile signals from the fingertips in object manipulation tasks," *Nature Rev. Neurosci.*, vol. 10, no. 5, pp. 345–359, 2009.

[11] U. H. Shah, R. Muthusamy, D. Gan, Y. Zweiri, and L. Seneviratne, "On the design and development of vision-based tactile sensors," *J. Intell. Robot. Syst.*, vol. 102, pp. 1–27, 2021.

[12] W. Yuan, R. Li, M.A. Srinivasan, and E. H. Adelson, "Measurement of shear and slip with a GelSight tactile sensor," in *Proc. IEEE Int. Conf. Robot. Automat.*, 2015, pp. 304–311.

[13] Y. She, S. Wang, S. Dong, N. Sunil, A. Rodriguez, and E. Adelson, "Cable manipulation with a tactile-reactive gripper," *Int. J. Robot. Res.*, vol. 40, no. 12-14, pp. 1385–1401, 2021.

[14] A. Grover, P. Nadeau, C. Grebe, and J. Kelly, "Learning to detect slip with barometric tactile sensors and a temporal convolutional neural network," in *Proc. IEEE Int. Conf. Robot. Automat.*, 2022, pp. 570–576.

[15] J. S. Son, E. A. Monteverde, and R. D. Howe, "A tactile sensor for localizing transient events in manipulation," in *Proc. IEEE Int. Conf. Robot. Automat.*, 1994, pp. 471–476.

[16] A. Vanarse, A. Osseiran, and A. Rassau, "A review of current neuromorphic approaches for vision, auditory, and olfactory sensors," *Front. Neurosci.*, vol. 10, 2016, Art. no. 171438.

[17] E. Donlon, S. Dong, M. Liu, J. Li, E. Adelson, and A. Rodriguez, "GelSlim: A high-resolution, compact, robust, and calibrated tactile-sensing finger," in *Proc. IEEE Int. Conf. Intell. Robots Syst.*, 2018, pp. 1927–1934.

[18] R. D. Howe and M. R. Cutkosky, "Sensing skin acceleration for slip and texture perception," in *Proc. IEEE Int. Conf. Robot. Automat.*, 1989, pp. 145–150.

[19] D. D. Damian, T. H. Newton, R. Pfeifer, and A. M. Okamura, "Artificial tactile sensing of position and slip speed by exploiting geometrical features," *IEEE/ASME Trans. Mechatron.*, vol. 20, no. 1, pp. 263–274, Feb. 2015.

[20] H. Chen et al., "Hybrid porous micro structured finger skin inspired self-powered electronic skin system for pressure sensing and sliding detection," *Nano Energy*, vol. 51, pp. 496–503, 2018.

[21] D. D. Damian, H. Martinez, K. Dermitzakis, A. Hernandez-Arieta, and R. Pfeifer, "Artificial ridged skin for slippage speed detection in prosthetic hand applications," in *Proc. IEEE Int. Conf. Intell. Robots Syst.*, 2010, pp. 904–909.

[22] M. Costanzo, G. De Maria, and C. Natale, "Detecting and controlling slip through estimation and control of the sliding velocity," *Appl. Sci.*, vol. 13, no. 2, 2023, Art. no. 921.

[23] Y. Chen, C. Prepscius, D. Lee, and D. D. Lee, "Tactile velocity estimation for controlled in-grasp sliding," *IEEE Robot. Automat. Lett.*, vol. 6, no. 2, pp. 1614–1621, Apr. 2021.

[24] M. R. Tremblay and M. R. Cutkosky, "Estimating friction using incipient slip sensing during a manipulation task," in *Proc. IEEE Int. Conf. Robot. Automat.*, 1993, pp. 429–434.

[25] B. Heyneman and M. R. Cutkosky, "Slip classification for dynamic tactile array sensors," *Int. J. Robot. Res.*, vol. 35, no. 4, pp. 404–421, 2016.

[26] N. Chavan-Dafle, R. Holladay, and A. Rodriguez, "Planar in-hand manipulation via motion cones," *Int. J. Robot. Res.*, vol. 39, no. 2-3, pp. 163–182, 2020.

[27] N. Doshi, O. Taylor, and A. Rodriguez, "Manipulation of unknown objects via contact configuration regulation," in *Proc. IEEE Int. Conf. Robot. Automat.*, 2022, pp. 2693–2699.

[28] Y. Karayiannidis, K. Pauwels, C. Smith, and D. Kragic, "In-hand manipulation using gravity and controlled slip," in *Proc. IEEE Int. Conf. Intell. Robots Syst.*, 2015, pp. 5636–5641.

[29] C. Wang, S. Wang, B. Romero, F. Veiga, and E. Adelson, "Swingbot: Learning physical features from in-hand tactile exploration for dynamic swing-up manipulation," in *Proc. IEEE Int. Conf. Intell. Robots Syst.*, 2020, pp. 5633–5640.

[30] T. Bi, C. Sferrazza, and R. D'Andrea, "Zero-shot sim-to-real transfer of tactile control policies for aggressive swing-up manipulation," *IEEE Robot. Automat. Lett.*, vol. 6, no. 3, pp. 5761–5768, Jul. 2021.

[31] D. Thompson, *Railway Noise and Vibration: Mechanisms, Modelling and Means of Control*. Amsterdam, The Netherlands: Elsevier, 2008.

[32] C. Gao, D. Kuhlmann-Wilsdorf, and D. D. Makel, "Fundamentals of stick-slip," *Wear*, vol. 162, pp. 1139–1149, 1993.

[33] A. Ajoudani et al., "Reflex control of the Pisa/IIT softhand during object slippage," in *Proc. IEEE Int. Conf. Robot. Automat.*, 2016, pp. 1972–1979.